Supplementary Information

Grafting Self-Assembled Monolayers on Polymeric Substrates toward Li_3N-stabilized Solid electrolyte Interphases

Juxin Yue,[a] Qibin Xie,[a] Ze Wang,[a] Ke Yue,[a] XingYao Zeng,[a] Cong Ma,[a] Hengyu Feng,[a] Peng Shi,[b] Shihui Zou,[a] Huadong Yuan,[a] Jianwei Nai,[a,c] Yao Wang,[a] Jianmin Luo,[a,c] Shaofei Wu,[d] Xinyong Tao[a,b,c]* and Yujing Liu[a,c]**

a. College of Materials Science and Engineering Zhejiang University of Technology Hangzhou 310014, P. R. China

b. Science and Education Integration College of Energy and Carbon Neutrality Zhejiang University of Technology Hangzhou 310014, P. R. China

c. State Key Laboratory of Green Chemical Synthesis and Conversion

d. Chilwee Power Group Co., Ltd. Huzhou 313100, P. R. China

* To whom correspondence should be addressed.
Email: sp24@zjut.edu.cn; tao@zjut.edu.cn; yujingliu@zjut.edu.cn

1. Experimental Section

1.1 Preparation of Self-Assembled Monolayers (SAMs) on PP Surface

Polypropylene (PP) separators (celgard 2500, JINGHONG NEW ENERGY) were pre-wetted with tert-butanol (99.9%, Macklin) and subsequently immersed in concentrated nitric acid (65.0~68.0%, Titan) for 10 minutes to introduce the active functional groups required for constructing SAMs. A solution of 7.0% (v/v) 3-aminopropyltrimethoxysilane (APTMS, 98.0%, Titan) in chloroform (99.0%, Titan) was prepared and stirred at 200 r/min for 30 minutes, yielding a hydrolyzed SAMs coating solution. The activated PP separator was then immersed in the coating solution for 3 minutes to complete the SAMs construction. The separator was dried for 12 hours at 45 °C. After drying, the separator was cut into 20 mm diameter discs and stored in a vacuum desiccator for further use.

1.2 Preparation of Lithium iron phosphate (LFP) cathode

First, LFP powder, Super P, and Polyvinylidene fluoride (PVDF) were dried at 90°C in the oven for 48 hours. The mass ratio of the components was 8:1:1. Subsequently, the materials were mixed and stirred in a homogenizer for 1 hour to obtain a uniform slurry. The slurry was then applied using a 100 μm scraper and dried in a vacuum oven at 60°C for 48 hours. The resulting LFP cathodes were punched into small discs with a diameter of 12 mm, with a mass loading of approximately 7 mg cm^{-2} for the LFP cathode. The rate in LFP | Li batteries is defined based on 1 C = 170 mAh g^{-1}.

1.3 Preparation of $LiNi_{0.8}Co_{0.1}Mn_{0.1}O_2$ (NCM 811) cathode

First, NCM 811 powder, Super P, and Polyvinylidene fluoride (PVDF) were dried in a 90°C oven for 48 hours. The mass ratio of the components was 8:1:1. Subsequently, the materials were mixed and stirred in a homogenizer for 1 hour to obtain a uniform slurry. The slurry was then applied using a 100 μm scraper and dried in a vacuum oven

at 60°C for 48 hours. The resulting NCM811 cathodes were punched into small discs with a diameter of 12 mm, with a mass loading of approximately 22 mg cm^{-2} for the NCM811 cathode. The rate in NCM811 | Li batteries is defined based on 1 C = 220 mAh g^{-1}.

1.4 Preparation of Liquid electrolyte (LE)

The electrolyte for Li | Cu, Li | Li, and LFP | Li cells consisted of a 1:1 volume ratio of 1,3-dioxolane (DOL) and dimethoxyethane (DME), with 1.0 M lithium bis(trifluoromethanesulfonyl)imide (LiTFSI) and 2 wt.% lithium nitrate ($LiNO_3$). The electrolyte for NCM 811 | Li cells contained a 1:1:1 volume ratio of diethyl carbonate (DEC), ethylene carbonate (EC), and dimethyl carbonate (DMC), with 1.0 M lithium hexafluorophosphate ($LiPF_6$) and 10 wt.% fluoroethylene carbonate (FEC).

1.5 Materials Characterization

Fourier Transform Infrared (FT-IR) spectroscopy was performed using a Nicolet 6700 spectrometer to investigate the grafting status of APTMS before and after cycling. The morphology and distribution of the SAMs were analyzed using Atomic Force Microscope based Infrared Spectroscopy (AFM-IR, Bruker-Dimension Icon IR). The surface morphology and microstructure of the separators, as well as the lithium deposition morphology, were observed via Scanning Electron Microscopy (SEM, Nova NanoSEM450). X-Ray photoelectron spectroscopy (XPS) (Thermo Scientific Nexsa) was performed to analyze the bonding form and grafting status of APTMS.

High-resolution XPS spectra were analyzed using Thermo Avantage software. Baseline subtraction was conducted by applying a smart background based on a modified Shirley method. Spectral deconvolution utilized a mixed Gaussian-Lorentzian function containing 30 percent Lorentzian and 70 percent Gaussian profiles. The full width at half maximum (FWHM) was restricted to a range of 0.5 to 1.6 eV to ensure reliable fitting results. All peak positions were calibrated against the adventitious C 1s peak at 284.8 eV.

1.6 Electrochemical Measurements

The ionic conductivity (σ) of the separators was evaluated using electrochemical impedance spectroscopy (EIS) on stainless steel (SS) | separator | SS symmetric cells. The measurements were conducted over a frequency range from 100 kHz to 0.1 Hz at room temperature. The ionic conductivity was calculated using the following equation:

$$\sigma = \frac{d}{R_b \times S}$$

where d is the thickness of the separator, R_b is the bulk resistance obtained from the high-frequency intercept on the real axis of the Nyquist plot, and S is the effective contact area of the SS electrode.

The lithium-ion transference number (t_{Li^+}) was determined using the Bruce–Vincent method in Li | separator | Li symmetric cells. The cell was subjected to a constant polarization voltage (ΔV) of 10 mV, and the current response was recorded until a steady state was reached. EIS was performed before and after the polarization. The t_{Li^+} was calculated according to the following equation:

$$t_{Li^+} = \frac{I_s(\Delta V - I_0 R_0)}{I_0(\Delta V - I_s R_s)}$$

where ΔV is the applied polarization voltage (10 mV), I_0 and I_s are the initial and steady-state currents, respectively, and R_0 and R_s are the initial and steady-state interfacial resistances, respectively.

1.7 Characterization of the SEI

Cyclic voltammetry (CV) measurements were performed using a CHI660 electrochemical workstation with a voltage range of 0 to 2.5 V to investigate the promoting effect of PP-APTMS on the decomposition of electrolyte components. The CV experiments were conducted using a two-electrode setup with the working electrode of Cu foil and the counter electrode of Li foil. And the separator is PP or PP-APTMS, respectively.

Electrochemical impedance spectroscopy (EIS) and the corresponding distribution of relaxation times (DRT) analysis were performed on Li | Li cells after

varying cycles (from 0 to 30 cycles) to assess the evolution of interfacial impedance.Electrochemical impedance spectroscopy (EIS) was performed on Li | Cu cells after varying cycles (from 0 to 100 cycles) to assess the evolution of interfacial impedance. XPS was employed to analyze the SEI on the surface of Li anodes in Li | Li half-cells assembled with PP and PP-APTMS after 20 cycles. All XPS spectra were processed using Avantage software. Contaminated carbon (C-C) was selected as the internal reference to correct the XPS data. The binding energy of 284.8 eV from the C-C peak was used for spectrum correction and to account for the charge effect. Additionally, the background was subtracted using the Tougaard method. The microstructure of the lithium deposits and the nanostructure of the Solid Electrolyte Interphase (SEI) were examined by Transmission Electron Microscopy (TEM), cryogenic-TEM (cryo-TEM, FEI Talos-S). Li | Cu half-cells with PP-APTMS separators were assembled, and lithium was plated onto a 150-mesh copper grid at a current density of 0.5 mA cm^{-2}, with a capacity of 0.5 mAh cm^{-2}. After deposition, excess material on the copper grid was washed with DOL in an Ar-filled glovebox, and the grid was transferred to a TEM sample holder for analysis in a TEM.

1.8 Electrochemical Performance Evaluation

Electrochemical performance was evaluated using a LANDT multichannel battery cycler. All coin cells (2032 type) were assembled and disassembled in an Ar-filled glovebox (H_2O < 0.01 ppm, O_2 < 0.01 ppm). Li | Cu, Li | Li, and Li | LFP cells were assembled with ether-based electrolytes, while Li | NCM 811 cells used ester-based electrolytes. Li | Cu half-cells were activated for the first three cycles between 0.01-1.0 V at a current density of 0.2 mA cm^{-2} to form a stable SEI. Lithium was then plated onto the copper current collector at a current density of 1 mA cm^{-2}, with an areal capacity of 1 mAh cm^{-2}, and stripped at the same current density until a cutoff voltage of 1.5 V was reached at room temperature. Li | Li symmetric cells were cycled at current densities of 1 mA cm^{-2} and 2 mA cm^{-2} at room temperature, with an areal capacity of 1 mAh cm^{-2}. Li | LFP full cells were activated for three cycles at 0.2 C to stabilize the SEI before cycling between 2.5 V and 3.8 V at a rate of 1 C. The electrochemical tests

were conducted using CR2032 coin cells assembled in an argon-filled glovebox (H_2O < 0.1 ppm and O_2 < 0.1 ppm). The electrolyte consisted of 1.0 M $LiPF_6$ in EC/DMC/FEC with a controlled volume of 50 μL per cell. The cell comprised a 100 μm-thick Li metal anode (diameter: 12 mm, area: 1.13 cm^2) and an NCM811 cathode with an areal loading of 22 mg cm^{-2} and active material content of 97%, yielding an N/P ratio of 4.8. A PP or PP-APTMS separator (diameter: 16 mm, slightly larger than the electrode) was employed to prevent short-circuiting. Prior to cycling, the assembled cells were rested for 8 hours to ensure complete electrolyte wetting. The formation protocol involved 0.1 C for 3 cycles and followed by 1.0 C between 2.8 V and 4.3 V for long-term cycling, and all electrochemical measurements were performed at 25°C. Constant current charge-discharge performance was assessed at room temperature using a LANDT battery testing system (CT-3001A1U).

1.8 Calculation method

Electrostatic potentials were calculated using the Materials Studio software package with DNP (double numerical with d and p polarization) basis sets. The convergence criteria for energy and force were set to 10^{-6} Ha and 2×10^{-3} Ha $Å^{-1}$, respectively. For the substrate modeling of SAMs, a PP molecule was used for the control group, while PP-APTMS was used for the experimental group (APTMS as the SAMs). A vacuum layer was constructed without any electrolyte components. Both models were constructed under identical conditions.

2. Supporting figure

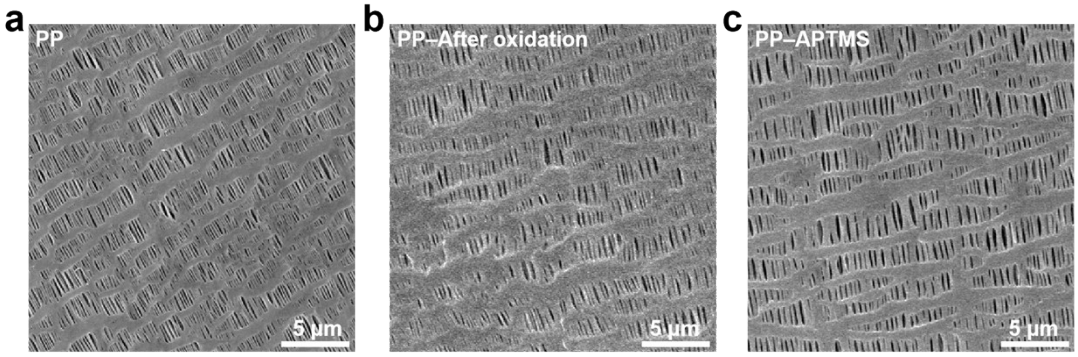

Figure S1. Top-view SEM images of (a) pristine PP, (b) oxidized PP, and (c) PP-APTMS separators.

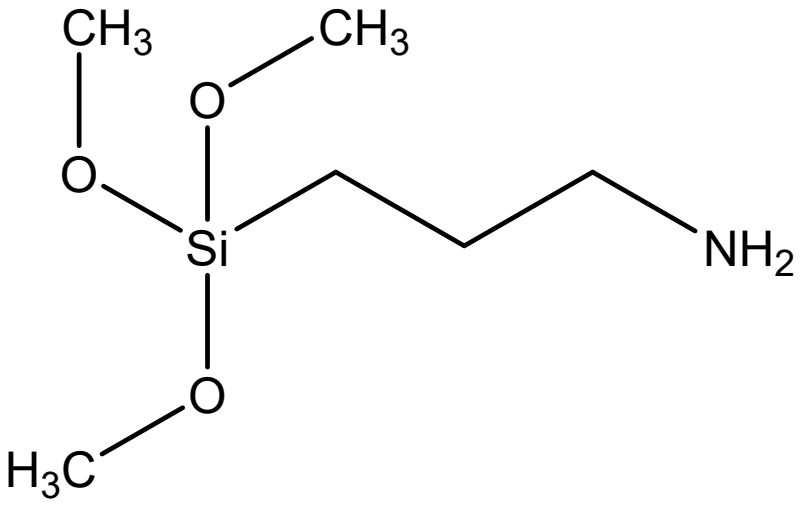

Figure S2 Molecular structure of APTMS

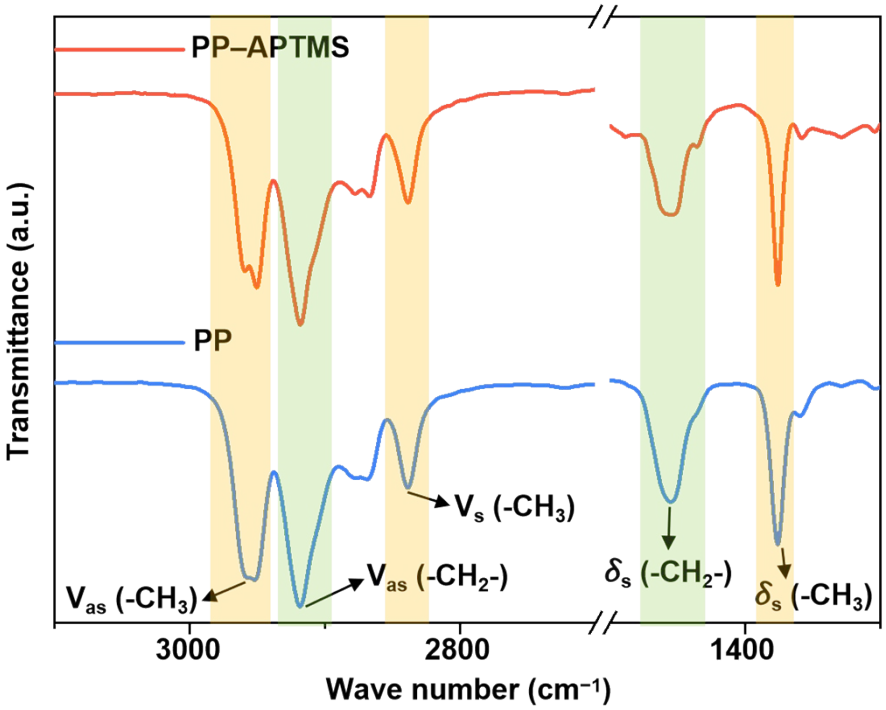

Figure S3. Enlarged FT-IR-ATR spectra corresponding to Fig. 1b, highlighting the characteristic vibrational features of the polypropylene (PP) backbone. The preserved C-H stretching and bending modes confirm that the structure of PP separator remains unchanged after surface modification.

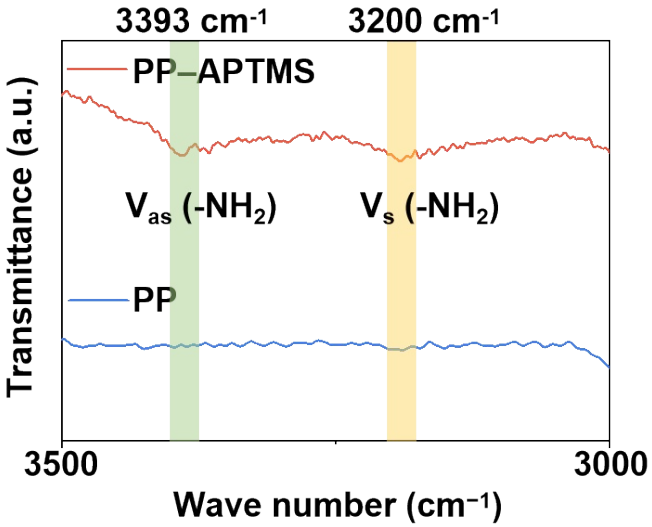

Figure S4. FT-IR spectra of the PP-APTMS separator in the range of 3500–3000 cm^{-1}.

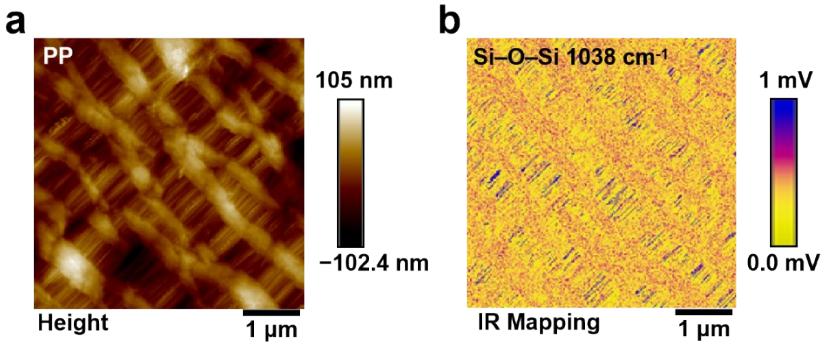

Figure S5. (a) AFM topography image and (b) corresponding Si-O-Si infrared mapping of the pristine PP separator.

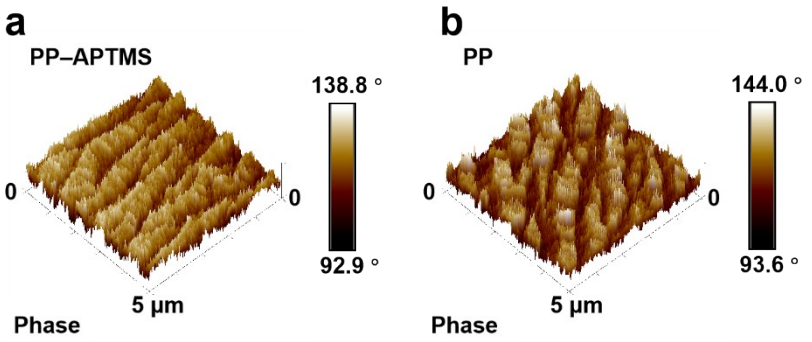

Figure S6. Phase images of (a) PP-APTMS and (b) PP separators.

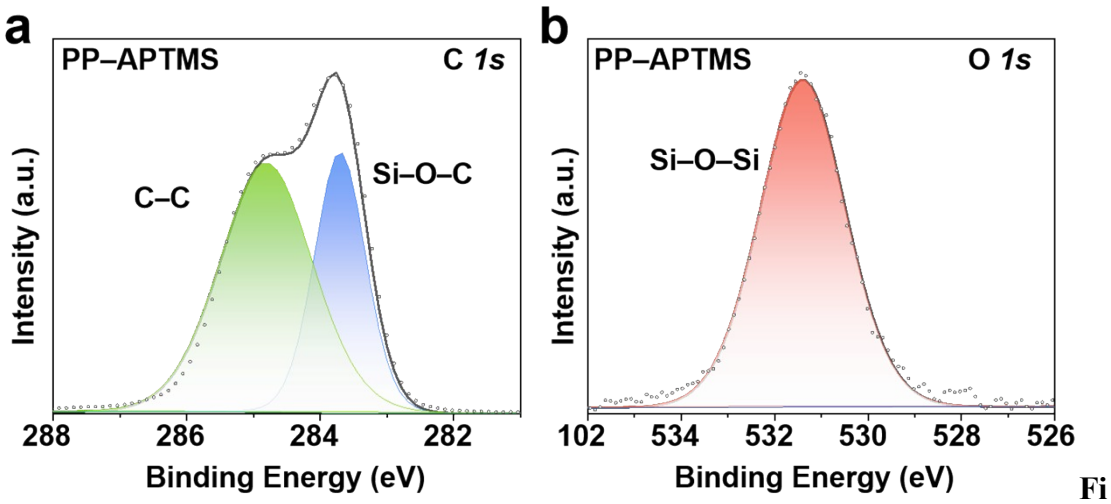

Figure S7. High-resolution XPS spectra of the PP-APTMS separator: (a) C 1*s* and (b) O 1*s*.

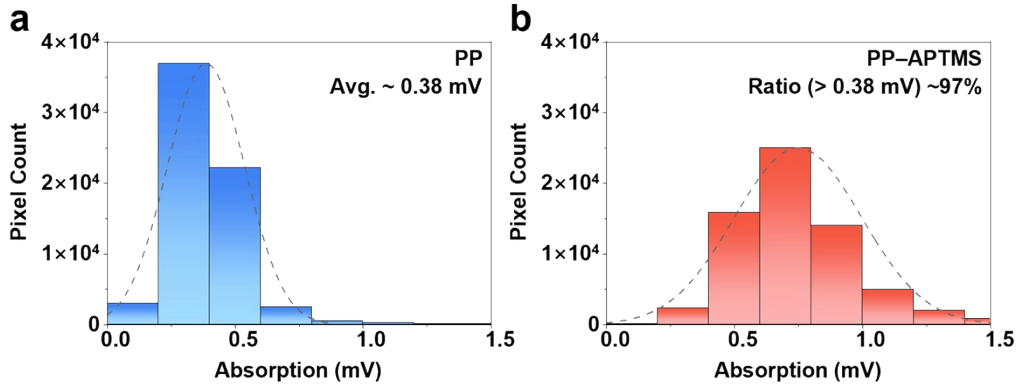

Figure S8. Statistical histograms of the Nano-IR absorption signal intensity and the corresponding Gaussian fitting curves for (a) the pristine PP and (b) the PP-APTMS separators.

The raw Nano-IR absorption mappings were collected at a resolution of 256 × 256 pixels. Using NanoScope Analysis 3.0 and OriginPro software, the raw signal intensity matrices (comprising 65536 independent spatial data points) into one-dimensional arrays for a global statistical evaluation were reshaped. On the basis of IR signal intensity distribution histograms fitted with Gaussian functions, the pristine PP separator surface exhibited an average background noise of approximately 0.38 mV.

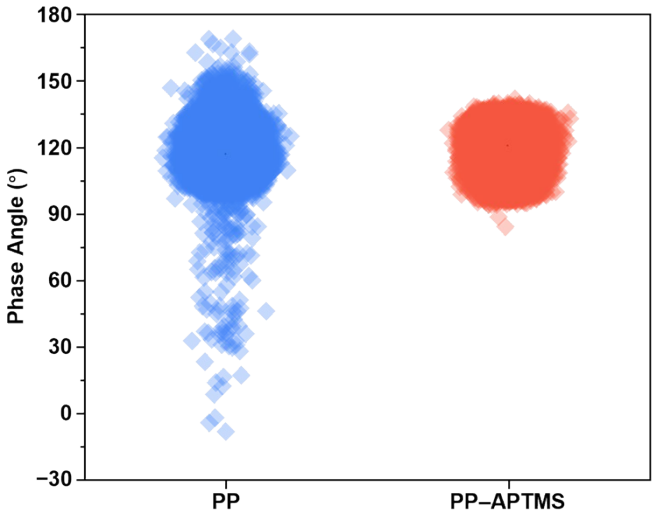

Figure S9. Statistical distribution of the phase angles for the pristine PP and PP-APTMS separators.

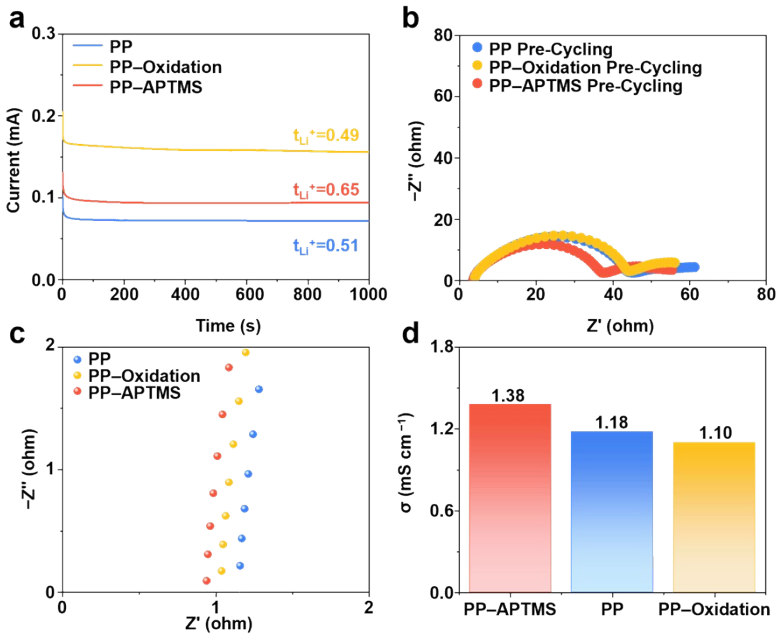

Figure S10. The t_{Li}^+, interfacial impedance, and ionic conductivities for the pristine PP, PP-Oxidation, and PP-APTMS separators. (a) The polarization curves of the Li | Li symmetric cells assembled with the three different separators. (b) Corresponding Nyquist plots of the symmetric cells with the three different separators. (c) Electrochemical impedance spectroscopy (EIS) profiles of the stainless steel (SS) | SS cells with the three separators. (d) Comparison of the calculated ionic conductivities for the three different separators.

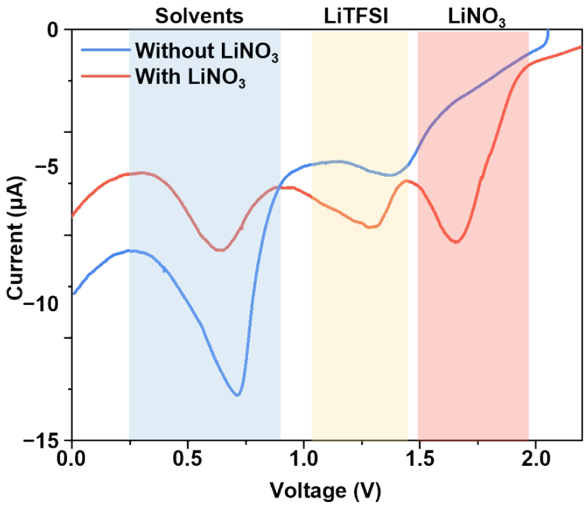

Figure S11. Cyclic voltammetry (CV) curve of the Cu | Li cell assembled with the pristine PP-APTMS separator.

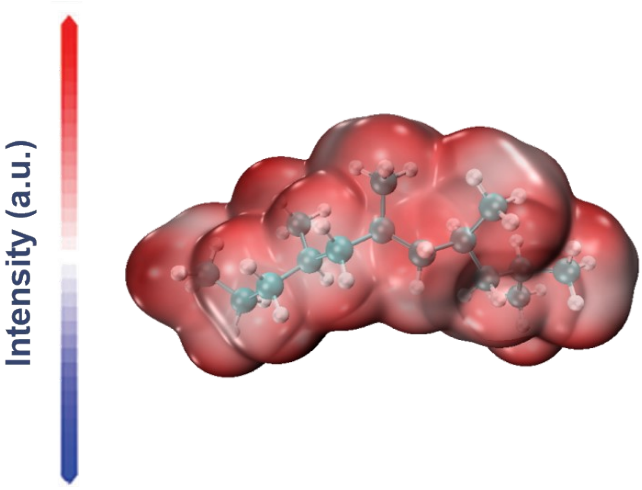

Figure S12. Electrostatic potential distribution of the pristine PP separator for comparison.

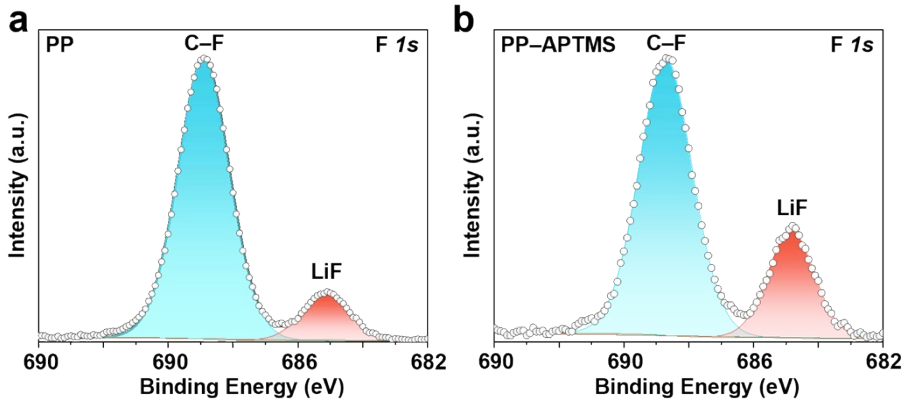

Figure S13. F 1s XPS spectra of Li | Li half-cells with PP and PP-APTMS separators after 20 cycles.

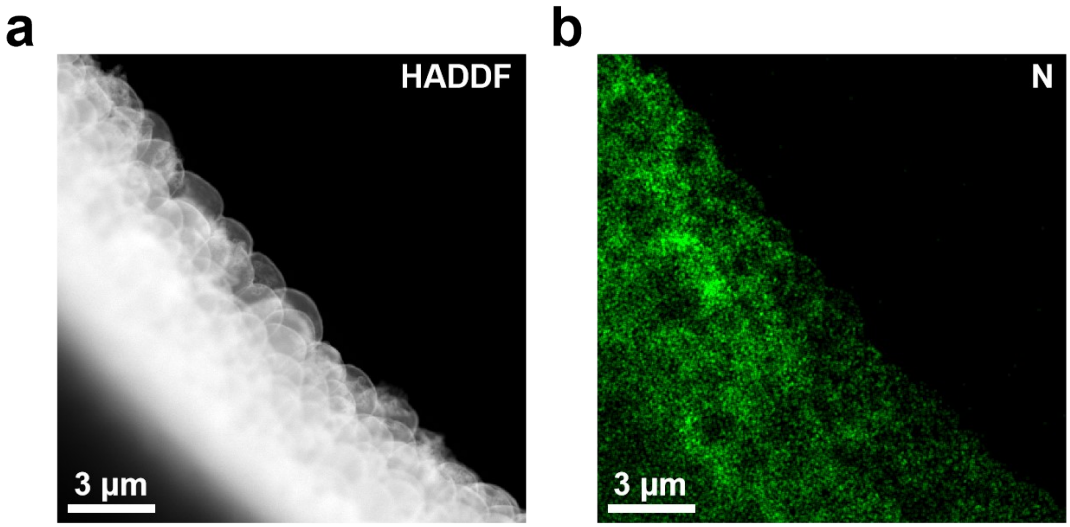

Figure S14. (a) HAADF-STEM image and (b) corresponding nitrogen (N) elemental mapping of the Li deposition with the PP-APTMS separator, corresponding to Fig. 3a.

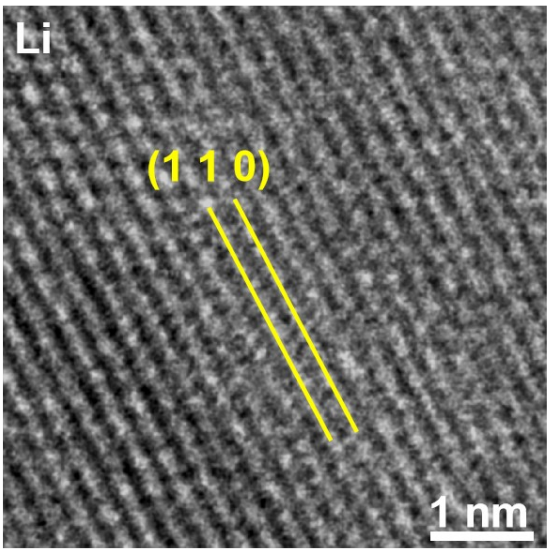

Figure S15. High-resolution TEM image and lattice spacing analysis of Li deposited on the PP-APTMS separator.

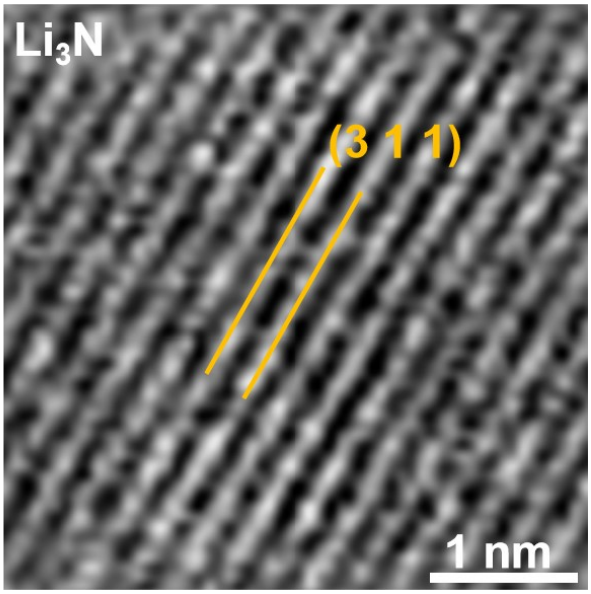

Figure S16. High-resolution TEM image and lattice spacing analysis of Li deposited on the PP separator.

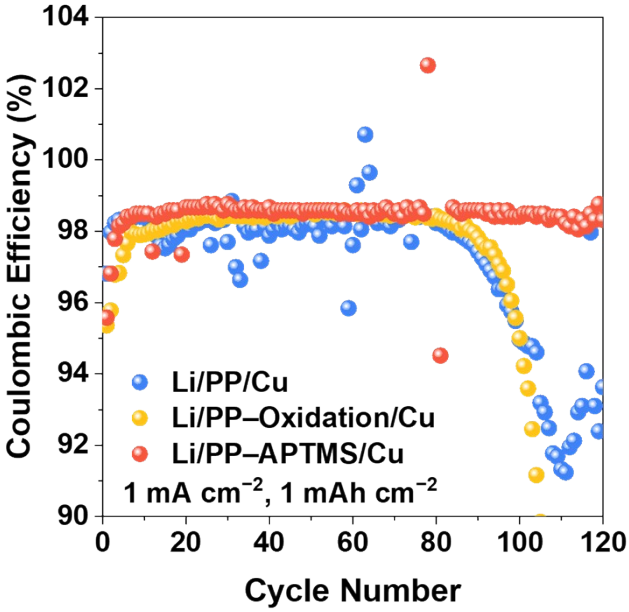

Figure S17. Coulombic efficiency of Li | Cu half-cells with PP, PP-Oxidation, PP-APTMS separators at 1.0 mA cm^{-2} and 1.0 mAh cm^{-2}.

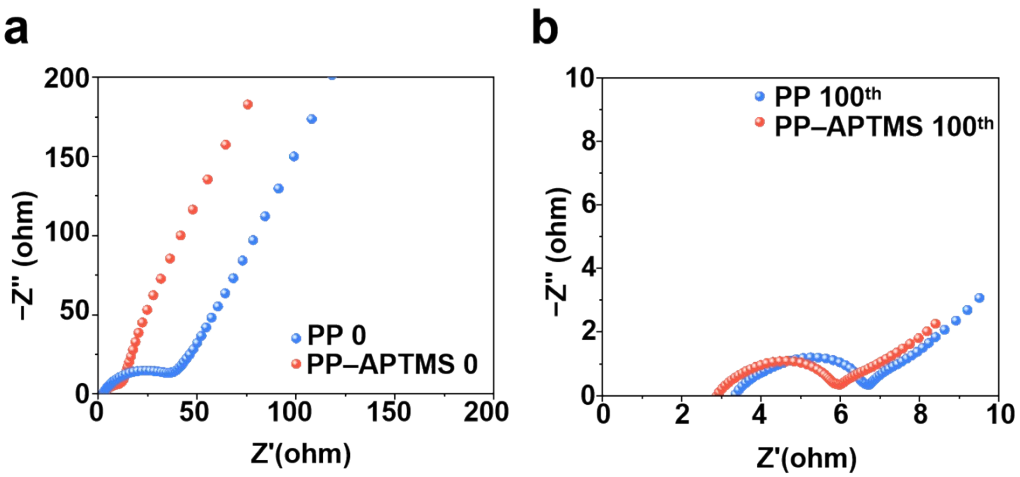

Figure S18. Electrochemical impedance spectra of Li | Cu half-cells with PP and PP-APTMS separators: (a) initial and (b) after 100 cycles.

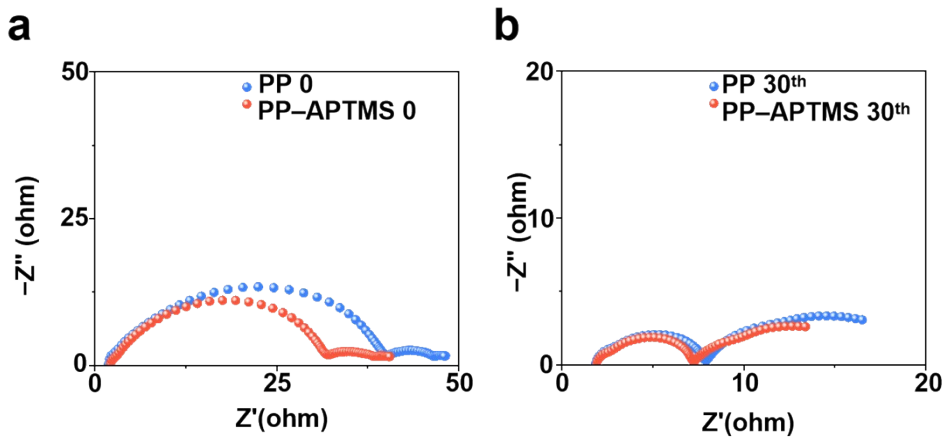

Figure S19. Electrochemical impedance spectra of Li | Li half-cells with PP and PP-APTMS separators: (a) initial and (b) after 30 cycles.

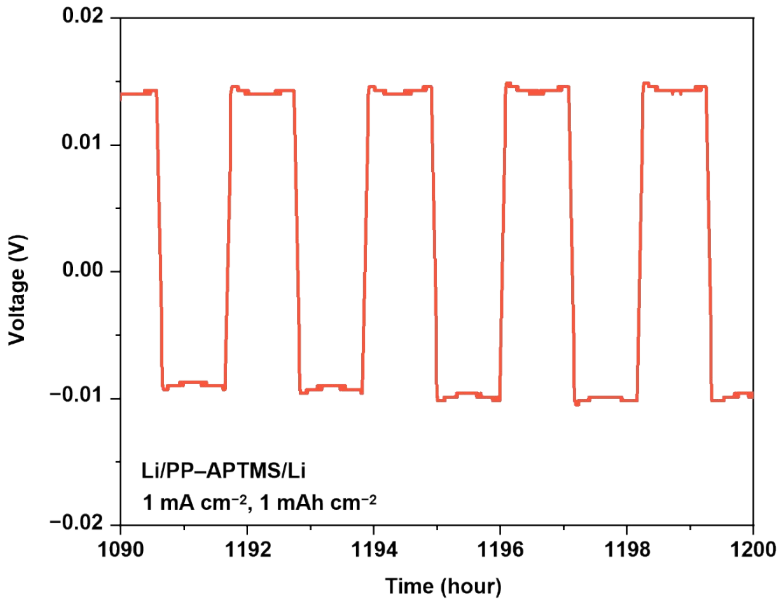

Figure S20. Enlarged voltage profiles of the Li | PP-APTMS | Li symmetric cell corresponding to Fig. 5a in the time range of 1090–1200 h at 1.0 mA cm^{-2} and 1.0 mAh cm^{-2}. The stable and continuous polarization without abrupt voltage drop confirms sustained Li plating/stripping without short-circuiting up to 1200 h.

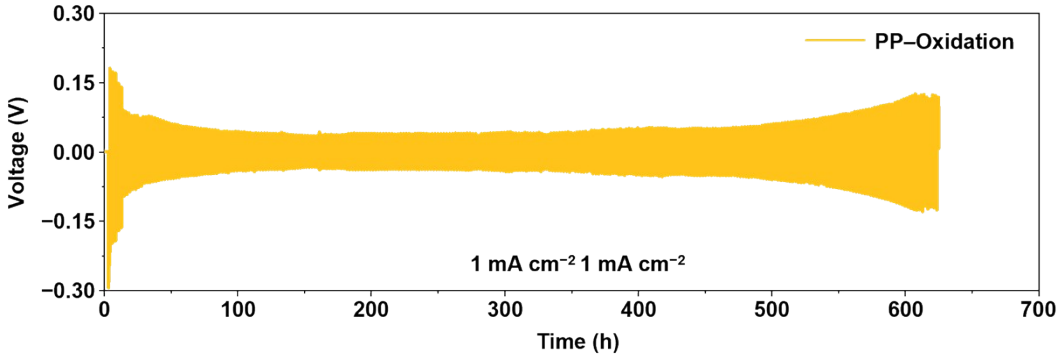

Figure S21. Voltage-time profiles of Li | Li symmetric cells with PP-Oxidation separators at 1 mA cm^{-2} and 1 mAh cm^{-2}.

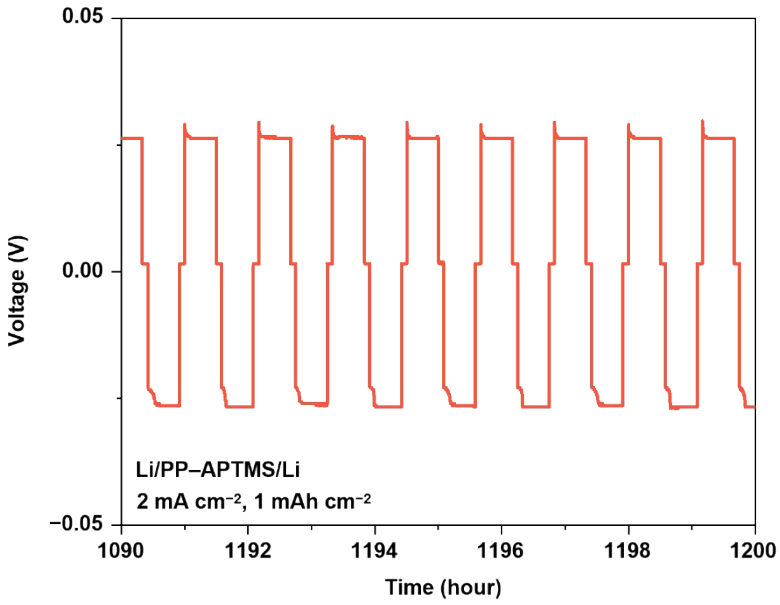

Figure S22. Enlarged voltage profiles of the Li | PP-APTMS | Li symmetric cell corresponding to Fig. 5b in the time range of 1090–1200 h at 2.0 mA cm^{-2} and 1.0 mAh cm^{-2}. The maintained low and steady polarization demonstrates stable cycling behavior without internal short-circuiting at prolonged cycling durations.

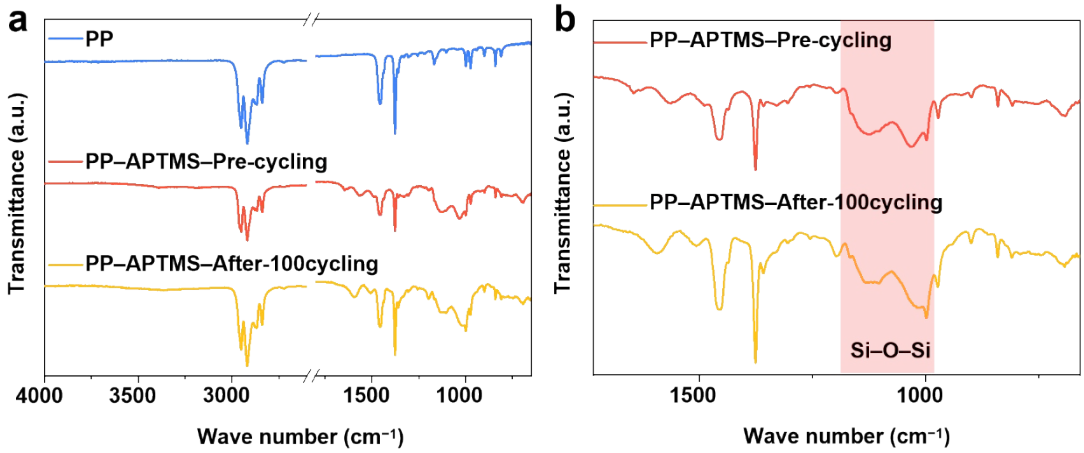

Figure S23. FT-IR spectra of PP-APTMS separators before cycling and after 100 cycles in Li | Li symmetric cells.

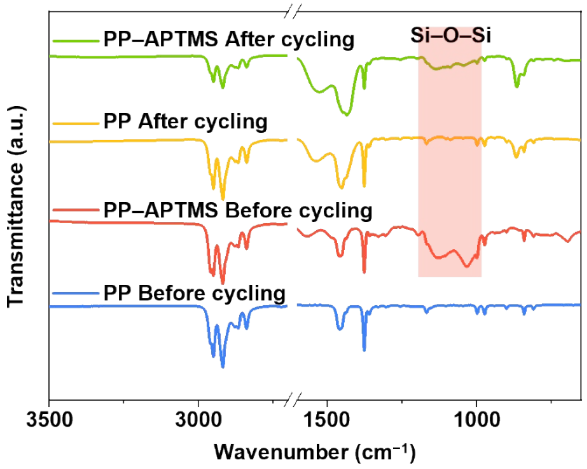

Figure S24. FT-IR spectra of the pristine PP and PP-APTMS separators before and after cycling in the ester-based electrolyte.

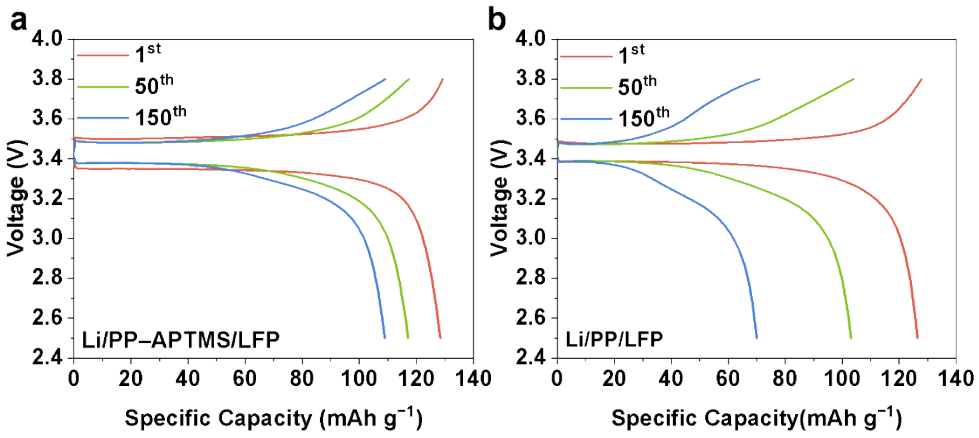

Figure S25. Charge–discharge profiles of Li | LFP full cells with PP and PP-APTMS separators at the 1st, 50th, and 150th cycle.

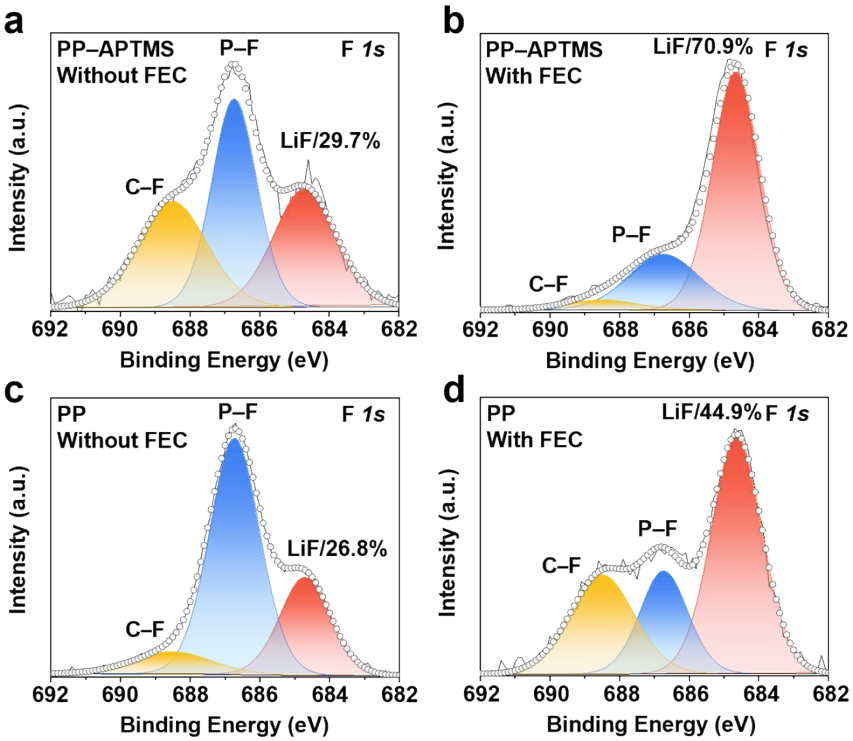

Figure S26. XPS spectra of the SEI on Li metal anodes harvested from Li | Li symmetric cells after 20 cycles. (a, b) the PP-APTMS separator and (c, d) the pristine PP separator with (a, c) FEC-free and (b, d) FEC-containing electrolyte.